IOP Publishing Journal of Optics
J. Opt. 20 (2018) 044005 (7pp) https://doi.org/10.1088/2040-8986/aaae52

Generalized Gilat–Raubenheimer method for density-of-states calculation in photonic crystals

Boyuan Liu[1], Steven G Johnson[2], John D Joannopoulos[3] and Ling Lu[1,4]

[1] Institute of Physics, Chinese Academy of Sciences/Beijing National Laboratory for Condensed Matter Physics, Beijing 100190, People's Republic of China
[2] Department of Mathematics, Massachusetts Institute of Technology, Cambridge, MA 02139, United States of America
[3] Department of Physics, Massachusetts Institute of Technology, Cambridge, MA 02139, United States of America

E-mail: linglu@iphy.ac.cn

Received 15 September 2017, revised 6 January 2018
Accepted for publication 9 February 2018
Published 5 March 2018

Abstract

An efficient numerical algorithm is the key for accurate evaluation of density of states (DOS) in band theory. The Gilat–Raubenheimer (GR) method proposed in 1966 is an efficient linear extrapolation method which was limited in specific lattices. Here, using an affine transformation, we provide a new generalization of the original GR method to any Bravais lattices and show that it is superior to the tetrahedron method and the adaptive Gaussian broadening method. Finally, we apply our generalized GR method to compute DOS of various gyroid photonic crystals of topological degeneracies.

Keywords: density of states, photonic crystal, topological photonics

(Some figures may appear in colour only in the online journal)

1. Introduction

Numerical methods of density of states (DOS) calculations [1] fall into two categories, extrapolation and interpolation. Each category can use linear or high-order fittings. Linear extrapolation methods include Gilat–Raubenheimer (GR) [2–6] and adaptive (Gaussian) broadening [7]. The high-order extrapolation methods were discussed in [8, 9]. Linear interpolation methods include the tetrahedron method [10–12], which does not need group-velocity information and is flexible in terms of volume grid division into tetrahedrons. The high-order interpolation methods were discussed in [13–15].

The extrapolation methods are better than the interpolation methods at band crossings [8, 16]. The interpolation methods interpolate the frequency (or energy) data from the nearest-neighbor momenta for linear interpolations and requires more neighboring data points for high-order interpolations. At the band crossings, interpolation methods sample the points across the degeneracy, resulting in the increase of errors. In contrast, an extrapolation method extrapolates the neighboring frequency data using both the frequency and the group velocity (first derivative) at each momentum point for linear extrapolations and requires higher-order derivatives for high-order extrapolations. Consequently, the extrapolation methods are not vulnerable to the band crossings while the interpolation methods are.

GR is the first linear extrapolation method proposed. It was originally formulated in the three-dimensional (3D) cubic grid and was extended to hcp [3], tetragonal [4] and trigonal lattices [5], by dividing the irreducible Brillouin zones (IBZ) into rectangular and triangular prisms. An improved GR method [6] derives the analytical formulation of the DOS contribution for parallelepiped subcells, applicable to all Bravais lattices. In this work, using a geometric transformation between a cube and a parallelepiped, we made a simpler generalization of the original GR method for all lattices. The

[4] This article belongs to the special issue: Emerging Leaders, which features invited work from the best early-career researchers working within the scope of the *Journal of Optics*. Professor Dr Ling Lu was selected by the Editorial Board of the *Journal of Optics* as an Emerging Leader

 © 2018 IOP Publishing Ltd Printed in the UK

convergence plots show that our generalized GR (GGR) method is consistently more accurate than the commonly-used tetrahedron and Gaussian methods. In appendix A, we showed that this GGR method is equivalent to the improved GR method derived in a different way. In appendix B, we discussed the GGR method for 2D.

In photonics, the GR method has never been adopted. The tetrahedron method [17] and histogramming [18–20] were used instead. A new method named Dirichlet-to-Neumann maps [21] has been implemented in 2D photonic crystals for finding both the DOS and the equifrequency surfaces. In this paper, we applied the GGR method to photonic crystals.

The rest of the paper is arranged in the following way. Section 2 introduces the details of this transformation for our GGR method. Section 3 compares the convergence of different methods. In section 4, we applied our method to topological photonic crystals. Section 5 discusses the computing efficiency of the GGR method. Section 6 concludes our findings.

2. Generalizing GR method by affine transformation

The core idea of our GGR method is to use an affine transformation [6] to transform a parallelepiped BZ into a cube, so that the original GR method can be used for any lattice. The BZ is a parallelepiped constituted by three reciprocal vectors $\mathbf{b}_i$ ($i = 1, 2, 3$), starting from an arbitrary point $\mathbf{k}_0$. The $\mathbf{k}$ points are uniformly distributed along three basis vectors $\mathbf{b}_i$. The affine transformation changes the $\mathbf{k}$-basis of the parallelepiped BZ into $\mathbf{t} = (t_1, t_2, t_3)$ of a cubic volume,

$$\mathbf{k} - \mathbf{k}_0 = B\mathbf{t} = \mathbf{b}_1 t_1 + \mathbf{b}_2 t_2 + \mathbf{b}_3 t_3, \tag{1}$$

where $t_1, t_2, t_3 \in [0, 1]$ and $B = [\mathbf{b_1}, \mathbf{b_2}, \mathbf{b_3}]$. Consequently the volume elements of the two sets of bases satisfies $\mathrm{d}V_k = \det(B)\mathrm{d}V_t = \Omega \mathrm{d}V_t$, in which Ω is the volume of the BZ.

We convert the DOS $[D(\omega)]$, the integral on equifrequency surface S_ω, from the $\mathbf{k}$ basis into the cubic $\mathbf{t}$ basis

$$D(\omega) = \frac{1}{\Omega}\sum_n \int_{S_\omega} \frac{\mathrm{d}S_k}{|\mathbf{v_k}|} = \sum_n \int_{S_\omega} \frac{\mathrm{d}S_t}{|\mathbf{v_t}|}, \tag{2}$$

since

$$\frac{1}{\Omega}\frac{\mathrm{d}S_k \mathrm{d}k_\perp}{|\mathbf{v_k}|\mathrm{d}k_\perp} = \frac{1}{\Omega}\frac{\mathrm{d}V_k}{\mathrm{d}\omega} = \frac{\mathrm{d}V_t}{\mathrm{d}\omega} = \frac{\mathrm{d}S_t \mathrm{d}t_\perp}{|\mathbf{v_t}|\mathrm{d}t_\perp}, \tag{3}$$

where $\mathbf{v_k}$ and $\mathbf{v_t}$ are the group velocities in each basis and $k_\perp$ and $t_\perp$ are the vectors normal to S_ω. n is the band index. $\mathbf{v_t}$ is obtained by scaling $\mathbf{v_k}$:

$$\mathbf{v_t} = \nabla_{\mathbf{t}}\omega(\mathbf{k}(\mathbf{t})) = \nabla_{\mathbf{k}}\omega \cdot \nabla_{\mathbf{t}}(B\mathbf{t}) = \mathbf{v_k} \cdot B, \tag{4}$$

where $\mathbf{v_k} \cdot B$ is a vector whose ith component is $(\mathbf{v_k} \cdot \mathbf{b}_i)$.

So far we have transformed the integral in parallelepiped BZ into integral in cubic volume $t_i \in [0,1]$. Then, we can use original GR method to calculate the DOS in the basis of t_i. The GR method partitions the cubic integral volume into uniform small cubes, with the $\mathbf{k}$ points at their centers. In each cubic subcell, we use linear extrapolation based on the frequency and group velocity of the central point to approximate the frequency of other region. In this case, the equifrequency surface of a given frequency is a polygon in each cubic cell. The area of the polygon is provided by the original GR method [2]. The final GGR formula is given in equation (A.4) in the appendix.

The integral region of our method is the whole BZ, a parallelepiped spanned by $\mathbf{b_1}$, $\mathbf{b_2}$, $\mathbf{b_3}$ or a fraction of it. This works for the general case for all lattices and symmetries. Although using IBZ is computationally more efficient, the choice of IBZ is symmetry specific. For example, we broke both the spatial and time-reversal symmetries in section 4, and the corresponding IBZ varies from case to case. When sampling the whole BZ, we recommend that the $\mathbf{k}$ mesh be shifted away from the BZ center (Γ) to avoid the divergence problem due to the zero group velocities [2].

3. Accuracy comparison between three methods

We compared the accuracy of GGR method with that of adaptive Gaussian broadening method and tetrahedron method. We assume that the lattice is body-centered cubic (bcc) and the BZ is a parallelepiped formed by three reciprocal lattice vectors $\mathbf{b}_i$ ($i = 1, 2, 3$ and $|\mathbf{b}_i| = 1$) starting from origin. The total number of $\mathbf{k}$ points is $N = N_1N_2N_3$, where N_i is the number of $\mathbf{k}$ points along the $\mathbf{b}_i$ direction, and for simplicity, we set $N_1 = N_2 = N_3$. The band frequency is $\omega = |\mathbf{k}|, |\mathbf{k}|^2, |\mathbf{k}|^3, |\mathbf{k}|^4$ respectively, so that we have analytical DOS to compare with. The error percentage is defined as:

$$\mathrm{Error}(N) = \frac{\int_0^1 |D_N(\omega) - D_\infty(\omega)|\mathrm{d}\omega}{\int_0^1 D_\infty(\omega)\mathrm{d}\omega}, \tag{5}$$

where $D_N(\omega)$ is the DOS calculated on N $\mathbf{k}$ points and $D_\infty(\omega)$ is the theoretical DOS.

In figure 1, error(N) of the three methods are presented in double logarithmic plots. The GGR method is better in the four cases. It is important to point out that, in the realistic band structures with band crossings, the tetrahedron interpolation method will have an even lower accuracy [8, 16]. Therefore, the GGR extrapolation method is a clear winner.

We fit the errors linearly $[\ln(\mathrm{error}(N)) = p_1 \ln(N) + p_2]$ for large number of $\mathbf{k}$ points, where p_1 and p_2 are the real fitting parameters. The power dependences of p_1 were tabulated in table 1 for all three methods. The p_1 values of GR method are consistent with the accuracy analysis in [22], which showed error(N) $\propto N^{-2/3}$. The p_1 values of the tetrahedron method are also close to the rate of convergence in [23].

We wrote the GGR method according to [2], the adaptive Gaussian broadening method following [7], and the tetrahedron method following [10, 12]. In our program of the adaptive Gaussian broadening method, width of Gaussian function is $\alpha|\mathbf{v_k}|\Delta k$, where Δk is the side length of a subcell. We set $\alpha = 1.0$, which is a dimensionless constant indicating

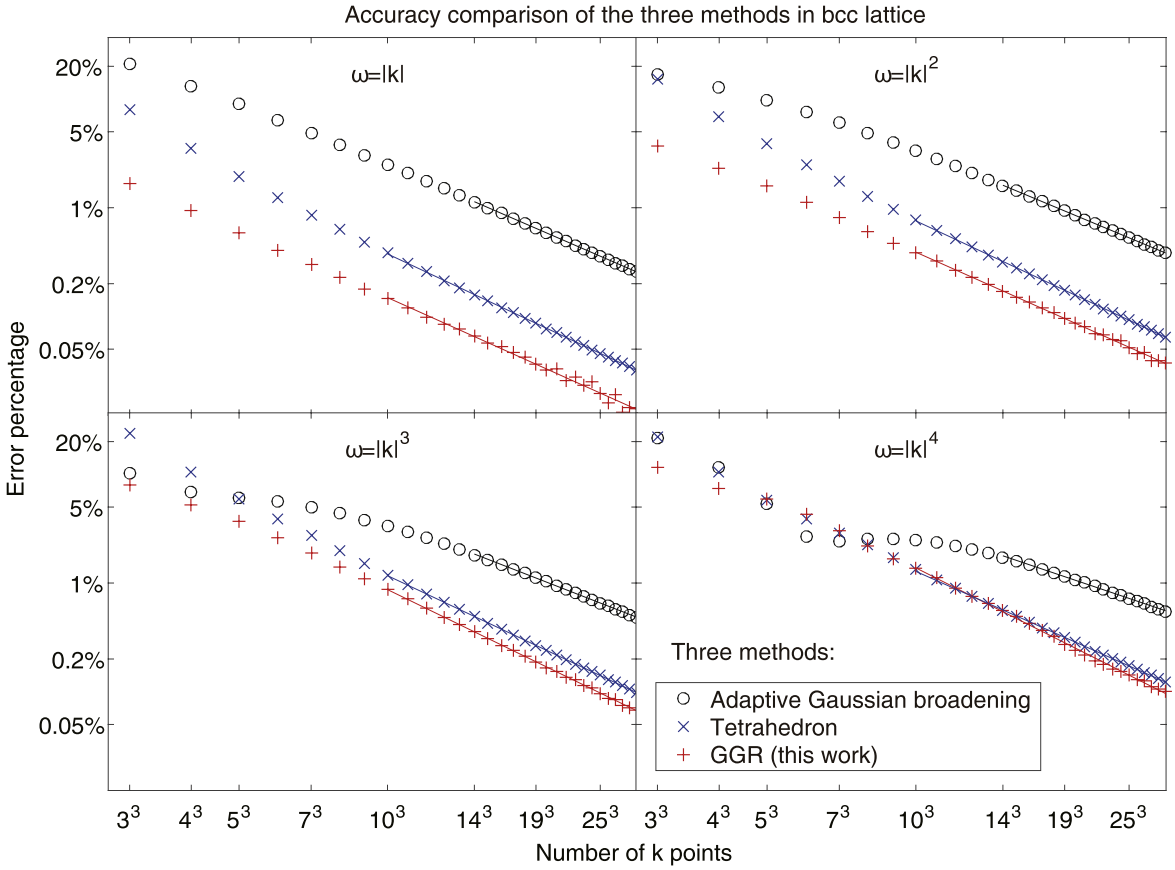

Figure 1. Error(N) of the three methods in bcc lattice in double-logarithmic plots. We assume that the band dispersion are $\omega = |\mathbf{k}|$, $|\mathbf{k}|^2$, $|\mathbf{k}|^3$, $|\mathbf{k}|^4$, respectively. The data we adopt to line fitting is from $N = 10^3$ to 32^3 for GGR and tetrahedron method and is from $N = 15^3$ to 32^3 for adaptive Gaussian broadening method. We note that the accuracy of tetrahedron method will be even worse in actual band structures with band crossings.

Table 1. The fitting parameters of adaptive Gaussian broadening, tetrahedron and our GGR method in figure 1.

p_1	$\omega = \lvert\mathbf{k}\rvert$	$\omega = \mathbf{k}^2$	$\omega = \lvert\mathbf{k}\rvert^3$	$\omega = \mathbf{k}^4$
Gaussian	−0.6545	−0.6314	−0.5882	−0.5118
Tetrahedron	−0.7067	−0.7059	−0.7103	−0.6712
GGR	−0.6786	−0.6757	−0.7353	−0.7625

the broadening level. We compared our GGR method program to the original GR method program 'GRINT' on CPC Program Library for simple cubic lattice. Our program of tetrahedron method was compared with the program 'tflovorn/ctetra' on github. In both methods, we got numerical consistence.

4. DOS of gyroid photonic crystals

Using the GGR method, we computed the DOS of six gyroid photonic crystals in figures 2(a)–(f), following the original designs from [24, 25] in which the DOS data were not presented. The insets are the real-space geometries in bcc unit cells. The band structures were calculated using MPB [26] for the frequencies and group velocities at 15^3 uniformly-distributed $\mathbf{k}$ points in the whole BZ.

Figure 2(a) is the single gyroid having a large band gap. Figure 2(b) is the double gyroid (DG) having a threefold quadratic degeneracy. The DOS around the degeneracy point, of frequency ω_0, shows a square-root relation of $D \propto |\omega - \omega_0|^{1/2}$. Figure 2(c) is the perturbed DG having a nodal ring. The DOS around the degeneracy line shows approximately a linear relation of $D \propto |\omega - \omega_0|$. Figure 2(d) is the parity ($\mathcal{P}$)-breaking DG having two pairs of Weyl points. Figure 2(e) is the time-reversal ($\mathcal{T}$)-breaking DG having one pair of Weyl points. Figure 2(f) is the $\mathcal{P}$-breaking DG having two pairs of Weyl points of the same frequency, in which the radius of the four defect air spheres is $r = 0.09a$. The DOS around the above Weyl points all shows a roughly quadratic relation of $D \propto |\omega - \omega_0|^2$.

5. Computing efficiency

Figure 1 shows that the extrapolative GGR method is more accurate than the interpolative tetrahedron method by utilizing

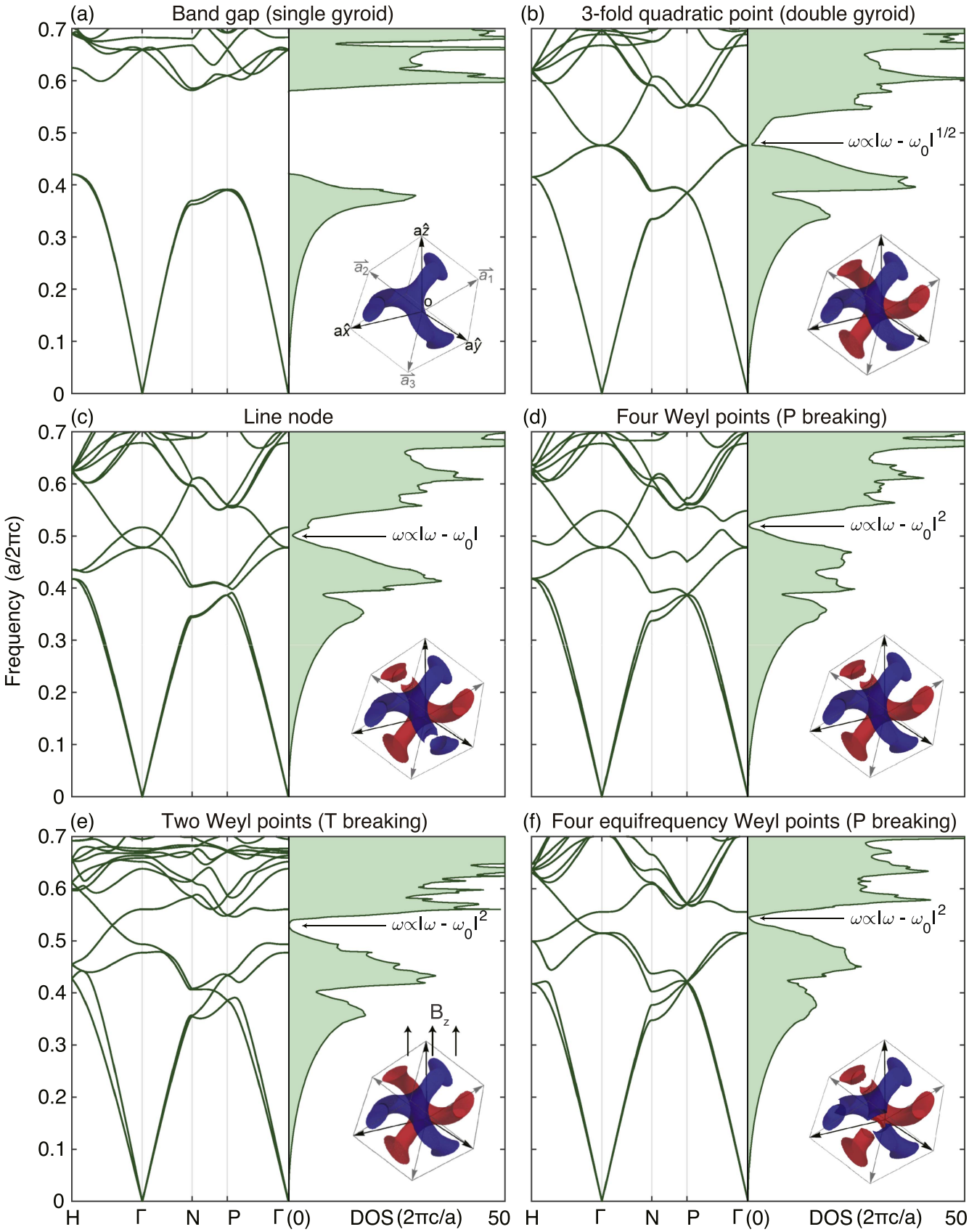

Figure 2. DOS of six gyroid photonic crystals. Gyroid photonic crystal with a band gap (a), a quadratic degeneracy point (b), a line node (c) and Weyl points (d)–(f). The designs of (a)–(e) are from [24] and the design of (f) is from [25]. Their dielectric constant is 16. Each inset shows the unit-cell geometry of the crystal whose air-sphere defects are enlarged (0.13a) in the illustration for the easy of identification, where a is the cubic lattice constant.

the extra data of group velocities, which requires extra computing time. Fortunately, the group velocities can be efficiently computed using the Hellman–Feynmann theorem $\frac{\partial\omega_{\mathbf{k}}}{\partial k_i} = \langle U_{\mathbf{k}}|\frac{\partial\hat{H}_{\mathbf{k}}}{\partial k_i}|U_{\mathbf{k}}\rangle$, where $|U_{\mathbf{k}}\rangle$ is the periodic part of the Bloch wave function and $\hat{H}_{\mathbf{k}}$ is the Hamiltonian operator of the system. Using MPB for example, the computation time for band dispersions with and without group velocities only differ by less than 2%. We note that the total computing time is proportional to the number of $\mathbf{k}$ points N, in which the time for computing DOS is negligible compared with the time for computing the band dispersions.

6. Conclusion

In summary, we generalized the GR method to all Bravais lattices using an affine transformation, which outperforms the tetrahedron and adaptive broadening methods. Our GGR method divides BZ into parallelepipeds and such an extrapolation method is advantageous in treating band crossings than interpolation methods. Future work includes high-order extrapolations [27] and more versatile sub-cell division. Our codes for the GGR and tetrahedron methods will be available for download at https://github.com/boyuanliuoptics/DOS-calculation.

Acknowledgments

We thank Tingtao Zhou for the initial efforts in this project and Hongming Weng and CT Chan for discussions. Boyuan Liu thanks Hao Lin and Qinghui Yan for their help on numerics. LL was supported by the National key R&D Program of China under Grant No. 2017YFA0303800, 2016YFA0302400 and by NSFC under Project No. 11721404. JDJ and SGJ was partly supported by the Army Research Office through the Institute for Soldier Nanotechnologies under contract no. W911NF-13-D-0001. SGJ was supported in part by the Air Force Research Laboratory under Agreement No. FA8650-15-2-5220.

Appendix A. Equivalence between GGR and improved GR method

Here, we prove that our GGR method is analytically equivalent to the improved GR method in [6]. In the improved GR method, the DOS contribution of one subcell is given by

$$\delta N = -\frac{1}{2}\frac{1}{B_1B_2B_3}\sum_{\sigma_1=0}^{1}\sum_{\sigma_2=0}^{1}\sum_{\sigma_3=0}^{1}(-1)^{\sigma_1+\sigma_2+\sigma_3} \times\left(A-\sum_{i=1}^{3}(-i)^{\sigma_i}B_i\right)^2\times\theta\left(A-\sum_{i=1}^{3}(-i)^{\sigma_i}B_i\right), \tag{A.1}$$

where $A=\omega-\omega_c$, $B_i=\frac{1}{2}\mathbf{v}\cdot\mathbf{b_i}\big/N_i(i=1,2,3)$, $\theta(x)$ is the Heaviside step function, ω_c is the frequency of central point of the subcell, $\mathbf{v}$ is the group velocity of this subcell, $\mathbf{b}_i$ is the reciprocal vector, N_i is the number of $\mathbf{k}$ points along the ith dimension and $N_1=N_2=N_3$.

In order to compare the expression (A.1) with that of our GGR method, we expand the above summation (A.1):

$$\begin{aligned}\delta N = &-\frac{1}{2}\frac{1}{B_1B_2B_3}\\ &\times\{[A-(B_1+B_2+B_3)]^2\theta(A-(B_1+B_2+B_3))\\ &+[A-(B_1-B_2-B_3)]^2\theta(A-(B_1-B_2-B_3))\\ &+[A-(-B_1+B_2-B_3)]^2\theta(A-(-B_1+B_2-B_3))\\ &+[A-(-B_1-B_2+B_3)]^2\theta(A-(-B_1-B_2+B_3))\\ &-[A-(-B_1-B_2-B_3)]^2\theta(A-(-B_1-B_2-B_3))\\ &-[A-(-B_1+B_2+B_3)]^2\theta(A-(-B_1+B_2+B_3))\\ &-[A-(B_1-B_2+B_3)]^2\theta(A-(B_1-B_2+B_3))\\ &-[A-(B_1+B_2-B_3)]^2\theta(A-(B_1+B_2-B_3))\}.\end{aligned} \tag{A.2}$$

Without loss of generality, we assume $A>0$ and $B_1\geqslant B_2\geqslant B_3\geqslant 0$. Then, expression (A.2) is transformed into a piecewise form,

$$\delta N=\begin{cases}\frac{B_0}{B_1} & B_1\geqslant B_2+B_3,\ 0\leqslant A\leqslant A_1\\ \frac{1}{B_1B_2B_3}[2(B_1B_2+B_2B_3+B_3B_1) & \\ \quad -(A^2+B_0^2)] & B_1\leqslant B_2+B_3,\ 0\leqslant A\leqslant A_1\\ \frac{1}{B_1B_2B_3}[(B_1B_2+3B_2B_3+B_3B_1) & \\ \quad -A(-B_1+B_2+B_3)-\frac{1}{2}(A^2+B_0^2)] & \\ \qquad A_1\leqslant A\leqslant A_2 & \\ \frac{2}{B_1B_2}[(B_1+B_2)-A] & A_2\leqslant A\leqslant A_3\\ \frac{1}{2B_1B_2B_3}[(B_1+B_2+B_3)-A]^2 & \\ \qquad A_3\leqslant A\leqslant A_4 & \\ 0 & A\geqslant A_4\end{cases}, \tag{A.3}$$

where

$$\begin{aligned}&B_0=(B_1^2+B_2^2+B_3^2)^{1/2},\ A_1=|B_1-B_2-B_3|,\\ &A_2=(B_1-B_2+B_3),\ A_3\\ &\quad=(B_1+B_2-B_3),\ A_4\\ &\quad=(B_1+B_2+B_3).\end{aligned}$$

Next, we get the expression of DOS contribution of our GGR method according to section 2,

$$\frac{\mathrm{d}S_t}{|\mathbf{v_t}|}=\begin{cases}\dfrac{4b^2}{v_{t1}} & v_{t1}\geqslant v_{t2}+v_{t3},\ 0\leqslant\Delta\omega\leqslant\omega_1\\ \dfrac{1}{v_{t1}v_{t2}v_{t3}}[2b^2(v_{t1}v_{t2}+v_{t2}v_{t3}+v_{t3}v_{t1}) & \\ \quad-(\Delta\omega^2+(v_tb)^2)] & \\ \quad\times v_{t1}\leqslant v_{t2}+v_{t3},\ 0\leqslant\Delta\omega\leqslant\omega_1\\ \dfrac{1}{v_{t1}v_{t2}v_{t3}}[b^2(v_{t1}v_{t2}+3v_{t2}v_{t3}+v_{t3}v_{t1}) & \\ \quad-b\Delta\omega(-v_{t1}+v_{t2}+v_{t3}) & \\ \quad-\dfrac{1}{2}(\Delta\omega^2+(v_tb)^2)] & \omega_1\leqslant\Delta\omega\leqslant\omega_2\\ \dfrac{2}{v_{t1}v_{t2}}[b^2(v_{t1}+v_{t2})-v_tb\Delta\omega] & \\ \qquad\omega_2\leqslant\Delta\omega\leqslant\omega_3 & \\ \dfrac{1}{2v_{t1}v_{t2}v_{t3}}[b(v_{t1}+v_{t2}+v_{t3})-\Delta\omega]^2 & \\ \qquad\omega_3\leqslant\Delta\omega\leqslant\omega_4 & \\ 0\quad\Delta\omega\geqslant\omega_4 & \end{cases},\qquad(A.4)$$

where $\Delta\omega=\omega-\omega_c$ and $v_t=|\mathbf{v_t}|$. $b=1/(2N_1)$ is half side length of subcell of the transformed cubic region. Similarly, we assume that $\Delta\omega>0$ and $v_{t1}\geqslant v_{t_2}\geqslant v_{t_3}\geqslant 0$, where $v_{ti}=\mathbf{v_k}\cdot\mathbf{b_i}$ is the component of transformed $\mathbf{v_t}$ $(i=1,2,3)$. And $\omega_1=b|v_{t1}-v_{t2}-v_{t3}|$, $\omega_2=b(v_{t1}-v_{t2}+v_{t3})$, $\omega_3=b(v_{t1}+v_{t2}-v_{t3})$, $\omega_4=b(v_{t1}+v_{t2}+v_{t3})$.

The expressions of DOS calculation from one subcell (B.1) and (A.4) are equivalent. They only differ by a constant which is $\mathrm{d}S_t/|\mathbf{v_t}|=\delta N/(8N_1N_2N_3)$.

Appendix B. GGR method in 2D

In order to use 3D GGR method for 2D lattices, we simply duplicate the frequency bands along a third imaginary dimension, so that the same GGR formulation applies with the following caveat.

In 3D, the DOS formula (A.4) is continuous (shown in figure 1 in [2]). However, for the extended 2D bands, the derivative of DOS is discontinuous due to $v_{t3}=0$, $\omega_1=\omega_2$ and $\omega_3=\omega_4$. Thus, the 2D formula becomes

$$\frac{\mathrm{d}S_t}{|\mathbf{v_t}|}=\begin{cases}\dfrac{4b^2}{v_{t1}} & 0\leqslant\Delta\omega\leqslant\omega_1\\ \dfrac{2}{v_{t1}v_{t2}}[b^2(v_{t1}+v_{t2})-v_tb\Delta\omega] & \omega_1\leqslant\Delta\omega\leqslant\omega_3\end{cases}\qquad(B.1)$$

whose first derivative is discontinuous at $\Delta\omega=\omega_1$. This discontinuity and the vanishing quadratic terms $(\Delta\omega^2)$ lead to a zigzag DOS plot. The zigzag behavior also exists in the tetrahedron method for the same reason, when being extended to 2D.

ORCID iDs

Boyuan Liu https://orcid.org/0000-0002-5108-5812

References

[1] Morris A J, Nicholls R J, Pickard C J and Yates J R 2014 Optados: a tool for obtaining density of states, core-level and optical spectra from electronic structure codes *Comput. Phys. Commun.* **185** 1477–85
[2] Gilat G and Raubenheimer L J 1966 Accurate numerical method for calculating frequency-distribution functions in solids *Phys. Rev.* **144** 390–5
[3] Raubenheimer L J and Gilat G 1967 Accurate numerical method of calculating frequency distribution functions in solids: II. Extension to hcp crystals *Phys. Rev.* **157** 586–99
[4] Kam Z and Gilat G 1968 Accurate numerical method for calculating frequency distribution functions in solids: III. Extension to tetragonal crystals *Phys. Rev.* **175** 1156
[5] Finkman E, Kam Z, Cohen E and Gilat G 1971 Accurate numerical method for calculating spectra in solids: IV. Extension to trigonal crystals *J. Phys. Chem. Solids* **32** 2423–7
[6] Bross H 1993 On the efficiency of different schemes for the evaluation of the density of states and related properties in solids *Phys. Status Solidi* b **179** 429–39
[7] Yates J R, Wang X, Vanderbilt D and Souza I 2007 Spectral and fermi surface properties from wannier interpolation *Phys. Rev.* B **75** 195121
[8] Pickard C J and Payne M C 1999 Extrapolative approaches to brillouin-zone integration *Phys. Rev.* B **59** 4685
[9] Pickard C J and Payne M C 2000 Second-order k p perturbation theory with vanderbilt pseudopotentials and plane waves *Phys. Rev.* B **62** 4383
[10] Lehmann G and Taut M 1972 On the numerical calculation of the density of states and related properties *Phys. Status Solidi* b **54** 469–77
[11] Jepson O and Anderson O K 1971 The electronic structure of hcp ytterbium *Solid State Commun.* **9** 1763–7
[12] Blöchl P E, Jepsen O and Andersen O K 1994 Improved tetrahedron method for brillouin-zone integrations *Phys. Rev.* B **49** 16223
[13] Methfessel M S, Boon M H and Mueller F M 1983 Analytic-quadratic method of calculating the density of states *J. Phys. C: Solid State Phys.* **16** L949
[14] Boon M H, Methfessel M S and Mueller F M 1986 Singular integrals over the brillouin zone: the analytic-quadratic method for the density of states *J. Phys. C: Solid State Phys.* **19** 5337
[15] Methfessel M S, Boon M H and Mueller F M 1987 Singular integrals over the brillouin zone: inclusion of k-dependent matrix elements *J. Phys. C: Solid State Phys.* **20** 1069
[16] Müller J E and Wilkins J W 1984 Band-structure approach to the x-ray spectra of metals *Phys. Rev.* B **29** 4331
[17] Busch K and John S 1998 Photonic band gap formation in certain self-organizing systems *Phys. Rev.* E **58** 3896
[18] Johnson P M, Koenderink A F and Vos W L 2002 Ultrafast switching of photonic density of states in photonic crystals *Phys. Rev.* B **66** 081102
[19] Nikolaev I S, Vos W L and Koenderink A F 2009 Accurate calculation of the local density of optical states in inverse-opal photonic crystals *J. Opt. Soc. Am.* B **26** 987–97
[20] Kano P, Barker D and Brio M 2008 Analysis of the analytic dispersion relation and density of states of a selected photonic crystal *J. Phys. D: Appl. Phys.* **41** 185106
[21] Liu V and Fan S 2011 Efficient computation of equifrequency surfaces and density of states in photonic crystals using Dirichlet-to-Neumann maps *J. Opt. Soc. Am.* B **28** 1837–43

[22] Gilat G 1972 Analysis of methods for calculating spectral properties in solids *J. Comput. Phys.* **10** 432–65
[23] Wiesenekker G and Baerends E J 1991 Quadratic integration over the three-dimensional brillouin zone *J. Phys.: Condens. Matter* **3** 6721
[24] Lu L, Fu L, Joannopoulos J D and Soljačić M 2013 Weyl points and line nodes in gyroid photonic crystals *Nat. Photon.* **7** 294–9
[25] Wang L, Jian S-K and Yao H 2016 Topological photonic crystal with equifrequency weyl points *Phys. Rev.* A **93** 061801
[26] Johnson S G and Joannopoulos J D 2001 Block-iterative frequency-domain methods for maxwell's equations in a planewave basis *Opt. Express* **8** 173–90
[27] Saye R I 2015 High-order quadrature methods for implicitly defined surfaces and volumes in hyperrectangles *SIAM J. Sci. Comput.* **37** A993–1019